Molecular Pharmacology Fast Forward. Published on May 13, 2015 as DOI: 10.1124/mol.115.098707
This article has not been copyedited and formatted. The final version may differ from this version.

Rotational symmetry of two pyrethroid receptor sites in the mosquito sodium channel

Yuzhe Du, Yoshiko Nomura, Boris S. Zhorov, Ke Dong

Department of Entomology, Genetics and Neuroscience Programs, Michigan State University, East Lansing, MI 48824, USA (Y.D., Y.N., K.D.)

Department of Biochemistry and Biomedical Sciences, McMaster University, Hamilton, Ontario, Canada (B.S.Z.)

Sechenov Institute of Evolutionary Physiology & Biochemistry, Russian Academy of Sciences, St. Petersburg (B.S.Z.)

Molecular Pharmacology Fast Forward. Published on May 13, 2015 as DOI: 10.1124/mol.115.098707
This article has not been copyedited and formatted. The final version may differ from this version.

Running title: Symmetry of Two Pyrethroid Receptors

Corresponding authors.

Email: dongk@cns.msu.edu; Telephone: 517-432-2034; Fax: 517-353-4354

Email: zhorov@mcmaster.ca; Telephone 1-905-525-9140 x. 22049; Fax: 1-905-522-9033

Number of text pages: 17

Number of tables: 2

Number of figures: 4

Number of references: 34

Number of words in Abstract: 245

Number of words in Introduction: 749

Number of words in Discussion: 1384

Nonstandard abbreviations: AaNa$_v$1–1, mosquito sodium channel from *Ae. aegypti*; DMT, deltamethrin; L45, linker connecting S4 and S5 of sodium channels; MC, Monte Carlo; MCM, Monte Carlo minimization; PMT, permethrin; PyR1, pyrethroid receptor site1; PyR2, pyrethroid receptor site 2.

Molecular Pharmacology Fast Forward. Published on May 13, 2015 as DOI: 10.1124/mol.115.098707
This article has not been copyedited and formatted. The final version may differ from this version.

Abstract

Voltage-gated sodium channels are the primary target of pyrethroid insecticides. Although it is well known that specific mutations in insect sodium channels confer knockdown resistance (kdr) to pyrethroids, the atomic mechanisms of pyrethroid-sodium channel interactions are not clearly understood. Previously, computer modeling and mutational analysis predicted two pyrethroid receptors, PyR1 (initial) and PyR2, located in the domain interfaces II/III and I/II, respectively. The models differ in ligand orientation and the number of transmembrane helices involved. Here we elaborated a revised PyR1 model of the mosquito sodium channel. Computational docking in the K_v1.2-based open channel model yielded a complex where a pyrethroid (deltamethrin) binds between the linker helix IIL45 and transmembrane helices IIS5, IIS6 and IIIS6 with its dibromoethenyl and diphenylether moieties oriented in the intra- and extracellular directions, respectively. The PyR2 and revised PyR1 models explained recently discovered kdr mutations and predicted new deltamethrin-channel contacts. Further model-driven mutagenesis identified seven new pyrethroid-sensing residues, three in the revised PyR1 and four in PyR2. Our data support the following conclusions: (i) each PyR is formed by a linker-helix L45 and three transmembrane helices (S5 and two S6s); (ii) IIS6 contains four residues that contribute to PyR1 and another four to PyR2; (iii) seven pairs of pyrethroid-sensing residues are located in symmetric positions within PyR1 and PyR2; and (iv) pyrethroids bind to PyR1 and PyR2 in similar orientations, penetrating deeply into the respective domain interfaces. Our study elaborates the dual pyrethroid-receptor sites concept and provides a structural background for rational development of new insecticides.

Molecular Pharmacology Fast Forward. Published on May 13, 2015 as DOI: 10.1124/mol.115.098707
This article has not been copyedited and formatted. The final version may differ from this version.

Introduction

Pyrethroid insecticides are extensively used for the control of insect pests and disease vectors involved in the transmission of various human diseases, including malaria and dengue ((WHO), 2007). Pyrethroids exert toxic effects by altering the gating of voltage-gated sodium channels (Narahashi, 1986; Bloomquist, 1996; Narahashi, 1996; Soderlund, 2010), which are essential for electrical signaling in the nervous system.

Like mammalian sodium channels, insect sodium channels comprise four homologous domains (I-IV), each having six membrane spanning helical segments (S1-S6) (Catterall, 2012; Dong et al., 2014). Segments S1-S4 in each domain constitute a voltage-sensing module, which is connected through a linker-helix (L45) to a pore-forming module. The pore module is composed of an outer helix S5, a pore-lining inner helix S6, and a membrane-reentrant P-loop from each domain. The pore module forms a central pore, while the four voltage-sensing modules are arranged around the pore module. In response to membrane depolarization, the S4 segments move outward, initiating opening of the activation gate formed by cytoplasmic parts of S6s (i.e., channel activation).

A major threat to the sustained use of pyrethroids in pest and vector control is the development of pyrethroid resistance. A well-known mechanism of pyrethroid resistance, knockdown resistance (kdr), is caused by naturally occurring sodium channel mutations (Soderlund, 2005; Davies et al., 2007; Rinkevich et al., 2013; Dong et al., 2014). The emerging pyrethroid resistance demands development of new insecticides. In the absence of X-ray structures of eukaryotic sodium channels, rational development of new pyrethroids can be facilitated by building homology models of insect sodium channels and computational docking of pyrethroids in these models.

The first pyrethroid receptor site model (O'Reilly et al., 2006) was elaborated for the house fly open sodium channel using the X-ray structure of a voltage-gated potassium channel

Molecular Pharmacology Fast Forward. Published on May 13, 2015 as DOI: 10.1124/mol.115.098707
This article has not been copyedited and formatted. The final version may differ from this version.

K_v1.2 (Long et al., 2005) as a template. According to this model, pyrethroids bind to the lipid-exposed interface formed by IIL45, which connects the second-domain transmembrane helices IIS4 and IIS5, the outer helix IIS5 and the inner helix IIIS6 (the IIL45-IIS5-IIIS6 triangle model). Hereafter we refer to this receptor as initial PyR1. Recently, we generated a model for a second pyrethroid receptor site, PyR2, in which ligands bind between helices IL45, IS5, IS6 and IIS6 (Du et al., 2013). We further suggested that simultaneous binding of pyrethroids to both PyR1 and PyR2 is required to effectively prolong the opening of sodium channels (Du et al., 2013). A common feature of both models is involvement of helices L45 and S5 from one domain in addition to the S6 helix from the neighboring domain. A distinguishing feature of PyR2 is involving of helix IS6 from the same domain I to which IL45 and IS5 belong. Due to the latter feature, pyrethroids are predicted to bind to PyR2 deeper (farther from lipids) than to initial PyR1 model. Another difference between the initial PyR1 model and PyR2 models is the opposite orientation of the bound pyrethroids. In particular, deltamethrin (DMT) is predicted to bind to the initial PyR1 model with its dibromoethenyl and diphenylether moieties oriented in the extra- and intra-cellular directions, respectively. In contrast, DMT is predicted to bind in PyR2 in a "reverse" orientation, with dibromoethenyl and diphenylether moieties oriented in the intra- and extra-cellular directions, respectively.

Earlier we demonstrated that a kdr mutation of valine to glycine (V1023G) in the middle of IIS6 (four positions downstream from the gating-hinge glycine) reduces the sensitivity of the $AaNa_v1$–1 sodium channel to pyrethroids (Du et al., 2013). This valine was not indicated as a pyrethroid-sensing residue in the initial PyR1 model (O'Reilly et al., 2006), but it is oriented towards the PyR1 suggesting that IIS6 be part of PyR1. Here we explored this possibility by docking DMT into a revised PyR1 model, which includes IIS6. We used our K_v1.2-based homology model of a mosquito sodium channel (Du et al., 2013) to simultaneously dock two DMT molecules to the channel. We propose a model of the sodium channel with two DMT

Molecular Pharmacology Fast Forward. Published on May 13, 2015 as DOI: 10.1124/mol.115.098707
This article has not been copyedited and formatted. The final version may differ from this version.

molecules where one ligand binds to PyR2 as we predicted before (Du et al., 2013), whereas another ligand binds quasi-symmetrically to the revised PyR1 model, between the linker helix IIL45 and transmembrane helices IIS5, IIS6 and IIIS6. Dibromoethenyl and diphenylether moieties of both DMT molecules are oriented in the intra- and extracellular directions, respectively. Subsequent model-driven mutagenesis followed by electrophysiological studies unveiled three new pyrethroid-sensing residues in the revised PyR1 model and four in PyR2. The PyR2 and revised PyR1 models display rotational quasi-symmetry around the pore axis and have many common features. Our study provides new insights into the concept of dual pyrethroid receptor sites and forms a structural background for rational development of new pyrethroid insecticides.

Materials and Methods

Computer modeling. The X-ray structure of the $K_v1.2$ channel (Long et al., 2005) was used as a template to build the open conformations of the $AaNa_v1$-1 channel. Sequence alignment of $K_v1.2$ and $AaNa_v1$-1 channels is shown in Figure 1. Homology modeling and ligand docking were performed using the ZMM program, see (Garden and Zhorov, 2010) and Monte Carlo-minimization protocol (Li and Scheraga, 1987) as described in our previous study (Du et al., 2013). Molecular images were created using the PyMol Molecular Graphics System, Version 0.99rc6 (Schrödinger, LLC, New York, NY).

Homology models of heterotetrameric asymmetric eukaryotic sodium channels are not expected to be as precise as X-ray structures of homotetrameric symmetric ion channels. Therefore, an apparent global minimum found through unbiased hands-free docking of a highly flexible ligand, like pyrethroids, is unlikely to correspond to the real structure of the ligand-channel complex. A solution to this problem is a biased docking of ligands to ligand-sensing residues, which are known from experiments. The biased docking involves distance constraints

Molecular Pharmacology Fast Forward. Published on May 13, 2015 as DOI: 10.1124/mol.115.098707
This article has not been copyedited and formatted. The final version may differ from this version.

between a ligand and ligand-sensing residues. When a specific ligand-channel distance in the model exceeds the upper distance constraint limit (which is usually set to 4 - 5 Å), a large energy penalty is added to the model energy. A Monte Carlo-minimization protocol modifies the model geometry and minimizes the penalty simultaneously with other energy terms, including van der Waals and electrostatic interactions. The distance constraints are considered to be satisfied when the constraints energy reaches zero. Further Monte Carlo minimization steps optimize the ligand-channel interactions. To preclude large deviations of the channel backbones from the X-ray templates (and thus preserve the channel folding), another set of distance constraints (pins) is set between matching alpha carbons in the template and the model. A pin constraint is a flat-bottom parabolic energy function that allows an atom (in this study, an alpha carbon) to deviate penalty free of up to 1 Å from the template and imposes a penalty of 10 kcal mol^{-1} $Å^{-1}$ for larger deviations. The pin constraints are necessary because the initial relaxation of an unconstrained homology model with a large ligand would cause significant deviations of the model backbones from the template due to steric clashes between the ligand and the protein.

Mutational data do not reveal specific atom-atom interactions between a ligand and a mutated sidechain. Therefore, during ligand docking we used "ligand-sidechain" constraints. Each such constraint specifies a ligand, a residue in the protein, and the targeted distance between the ligand and the residue sidechain, which was set to 5 Å. Each constraint instructed the ZMM program to choose a closest pair of atoms between the ligand and specific sidechain and apply a distance constraint to these atoms. The closest pairs of atoms are selected in the beginning of each energy minimization, thus allowing modification of atom-atom constraints during the MCM search for the apparent global minimum.

To overcome the problem of different residue numbers in homologous positions of sodium channels in different organisms and to highlight symmetric locations of residues in

Molecular Pharmacology Fast Forward. Published on May 13, 2015 as DOI: 10.1124/mol.115.098707
This article has not been copyedited and formatted. The final version may differ from this version.

different channel domains, we used a residue-labeling scheme, which is universal for P-loop channels (Zhorov and Tikhonov, 2004; Du et al., 2013). A residue label includes the domain number (1– 4), segment type (k, the linker-helix L45; i, the inner helix S6; and o, the outer helix S5), and relative number of the residue in the segment, see Figure 1.

Site-directed mutagenesis. We used a mosquito sodium channel, $AaNa_v1$-1, from *Ae aegypti* to generate all mutants used in this study. Site-directed mutagenesis was performed by Polymerase Chain Reaction (PCR) using Pfu Turbo DNA polymerase (Stratagene, La Jolla, CA). All mutagenesis results were confirmed by DNA sequencing.

Expression of $AaNa_v$ channels in *Xenopus* oocytes and electrophysiology. Procedures for preparation of oocytes and cRNA and injection were identical to those described previously (Tan et al., 2005). Methods and data analysis for two-electrode voltage clamp recording of sodium currents and measurement of tail currents induced by pyrethroids were identical to those previously described (Tatebayashi and Narahashi, 1994; Tan et al., 2005). All experiments were performed at room temperature. Sodium currents were measured with an OC725C oocyte clamp (Warner Instruments, Hamden, CT) and a Digidata 1440A interface (Axon Instruments Inc., Foster City, CA), pCLAMP 10.2 software (Axon Instruments Inc.) was used for data acquisition and analysis.

Statistical analysis.

Results are reported as mean ± S.E.M. Statistical significance was determined by using one-way analysis of variance with Scheffe's post hoc analysis, and significant values were set at $p < 0.05$.

Chemicals.

DMT was kindly provided by Dr. Ralf Nauen (Bayer CropScience AG). Permethrin (PMT) was purchased from ChemService. Pyrethroids were dissolved in dimethyl sulfoxide (DMSO) in a 100 mM stock. The working concentrations were prepared in ND96 recording solution

Molecular Pharmacology Fast Forward. Published on May 13, 2015 as DOI: 10.1124/mol.115.098707
This article has not been copyedited and formatted. The final version may differ from this version.

immediately prior to experiments. The concentration of DMSO in the final solution was <0.5%, which had no effect on the function of sodium channels.

Results

Docking two deltamethrin molecules in the AaNa$_v$1-1 channel model. As a starting point we used our AaNa$_v$1-1 model with DMT bound to PyR2 (Du et al., 2013). In this model the dibromoethenyl and diphenylether moieties of DMT are oriented, respectively, in the intra- and extracellular directions, while the bulky, rigid dimethylcyclopropane fragment fits between helices IL45, IS5, IS6, and IIS6 (Fig. 2A). We placed the second DMT molecule between helices IIL45, IIS5, IIS6 and IIIS6 (Fig. 2B) and set the ligand starting conformation and orientation as for DMT in PyR2. We further imposed two ligand-sidechain distance constraints involving most separated PyR1 residues, L^{2k7} (Usherwood et al., 2007) and V^{2i18} (Du et al., 2013), and performed three stages of MC-minimization. In the first stage, the channel backbones and the ligands' bond angles were kept rigid to avoid their large deformations due to very strong repulsion with the ligand that was manually placed into PyR1. At the second stage, all the torsional and bond angles were allowed to vary, but pins and the ligand-sidechain constraints were preserved. This stage yielded a low-energy structure in which the distance constraints were satisfied and both DMT molecules had only attractive (negative-energy) interactions with the channel residues. In the third stage all the constraints were removed. The energy further decreased, while the DMT-channel geometry changed insignificantly. In particular, none of the alpha carbons deviated more than 1.5 Å from the respective template positions.

The ternary complex of AaNa$_v$1-1 with two DMT molecules is shown in Fig. 2 C,D. Both ligands bind into respective domain interfaces and interact with the channel residues, many of

Molecular Pharmacology Fast Forward. Published on May 13, 2015 as DOI: 10.1124/mol.115.098707
This article has not been copyedited and formatted. The final version may differ from this version.

which are in symmetric positions (Fig. 1). Orientation of the two DMT molecules, which are bound to PyR2 and revised PyR1 models, are similar but not identical (Fig. 2 A,B). Both DMT molecules bind deeply in domain interfaces (Fig. 2 C,E,F), while their terminal aromatic rings approach the inner pore without blocking the ion permeation (Fig. 2D). A total of two linker-helices (L45) and five transmembrane helices (S5 and S6) contribute to PyR1 and PyR2. Among these only IIS6 is a part of both receptor sites, contributing four residues to PyR1 and six residues to PyR2 (Fig. 2D). One face at the extracellular half of IIS6 contributes to PyR2, whereas the opposite face in the intracellular half of the helix contributes to PyR1 (Fig. 2D). The only exception is the pore-facing residue F^{2i22} that is close to the terminal aromatic rings of the ligands bound to PyR1 and PyR2 (Fig. 2D). In both ligands, the bulky dimethylcyclopropyl moiety fits in the kink region between a linker helix L45 and the outer helix S5. The nitrile group approaches a conserved asparagine in position *i20* (S6) and its putative open-state H-bonding partner in position *i29* of the preceding domain (Tikhonov et al., 2015). The predictability of our model was tested by mutational analysis as described below.

Mutational analysis confirmed new pyrethroid-sensing residues in PyR1 and PyR2. Our model of the $AaNa_v1$-1 sodium channel with DMT molecule bound to PyR1 is consistent with published experimental data, which describe pyrethroid-sensing residues L^{2k7}, M^{2k11}, L^{2o6}, V^{2i18}, F^{3i13}, F^{3i16}, F^{3i17}, and N^{3i20} (see Fig. 3, Table 1 and references therein). Among these eight previously known contributors to PyR1, mutations of five residues have been identified in pyrethroid-resistant populations as kdr mutations: $M^{2k11}T$, $L^{2o6}I$, $V^{2i18}G$, $F^{3i13}C$, and $F^{3i17}I$ (Guerrero et al., 1997; He et al., 1999; Morin et al., 2002; Brengues et al., 2003; Kawada et al., 2009). Our PyR2 model (Du et al., 2013) described five pyrethroid-sensing residues (I^{1k7}, V^{1k11}, L^{1i18}, I^{2i13}, and L^{2i16}) and intensive MC-minimization of the channel model with two DMT molecules did not reveal any conflict between the ligands bound to PyR1 and PyR2, thus confirming our PyR2 model (Du et al., 2013).

Molecular Pharmacology Fast Forward. Published on May 13, 2015 as DOI: 10.1124/mol.115.098707
This article has not been copyedited and formatted. The final version may differ from this version.

Importantly, the analysis of the channel model with two DMT molecules revealed ten residues which interact with the bound ligands (Fig. 3 A,B), but have not been previously described as components of PyR1 or PyR2. These ten residues include three residues in PyR1 (F^{2i22}, L^{2i25} and L^{2i26}) and seven residues in PyR2 (S^{1o2}, L^{1o6}, I^{1i22}, I^{1i25}, S^{1i29}, N^{2i15} and N^{2i20}). Mutations of three out of the ten residues, N^{2i15}S, F^{2i22}S, and L^{2i26}A, have been previously associated with pyrethroid resistance: N^{2i15}S from *Anopheles sinensis* (Tan et al., 2012); F^{2i22}S from *Blattella germanica* (Pridgeon et al., 2002) and *Plutella xylostella* (Endersby et al., 2011); and L^{2i26}V from *Tetranychus urticae* (Kwon et al., 2010). We mutated the ten pyrethroid-sensing residues in PyR1 and PyR2, as well as some residues beyond PyR1 and PyR2 and explored the actions of DMT and PMT on the mutants. For known kdr mutants, we tested the amino acid substitutions identified in resistant insects (e.g. F^{2i22}S), whereas for new model-predicted pyrethroid-sensing residues we evaluated alanine substitutions.

A total of 17 single mutants and two double mutants of the $AaNa_v1$-1 channel were investigated. All mutant channels generated sufficient sodium currents in *Xenopus* oocytes for further functional analysis. With only a few exceptions, most mutant channels showed insignificant changes in gating properties (voltage dependence of activation and fast inactivation) when compared to wild-type channels (Table 2). However, channels incorporating the L^{1o6}A mutation displayed dramatic hyperpolarizing shifts in the voltage-dependence of both activation and inactivation. In addition, mutations I^{1i25}A and L^{2i26}A each caused hyperpolarizing shifts (~14 and 10 mV, respectively) in the voltage dependence of inactivation in $AaNa_v1$-1 channels (Table 2).

To evaluate channel sensitivity to pyrethroids, the percentage of sodium channels modified by DMT or PMT was determined by the method developed by Tatebayashi and Narahashi (Tatebayashi and Narahashi, 1994). Results of these experiments are shown in Fig. 4. We observed strong reduction of sensitivity with mutation of three residues within PyR1

Molecular Pharmacology Fast Forward. Published on May 13, 2015 as DOI: 10.1124/mol.115.098707
This article has not been copyedited and formatted. The final version may differ from this version.

($F^{2i22}S$, $L^{2i25}A$ and $L^{2i26}A$) and four within PyR2 ($S^{1o2}A$, $I^{1i22}A$, $S^{1i29}A$ and $N^{2i15}S$) to both DMT and PMT. These results confirm the model-predicted pyrethroid-sensing residues in both PyR1 and PyR2 models. In particular, our experiments confirmed that the revised PyR1 model includes helix IIS6, which was not a part of the initial PyR1 model (O'Reilly et al., 2006).

Our data show generally similar effects of mutations on the action of DMT and PMT (Fig. 4) suggesting that both ligands bind rather similarly to respective receptor sites. It should be noted that mutational analysis cannot demonstrate specific interactions of individual DMT moieties with individual chemical groups of the mutated residues. Therefore we refrained in this study from docking PMT to PyR1 or PyR2. Our model of the channel with PMT bound to PyR2 is available elsewhere (Du et al., 2013). An approach to address the challenging problem of atomic details of ligand-channel interactions should involve exploration of action of different pyrethroids on different mutants. This massive task is beyond the goal of our current study.

Effect of mutations beyond PyR1 and PyR2. Residues N^{1o5} and R^{1o7} are located around the predicted PyR2, but do not interact with pyrethroids in our model. In agreement with the model, mutations $N^{1o5}A$ and $R^{1o7}A$ had but small effects on the action of pyrethroids (Fig. 4).

Glycine G^{1k9} in the IL45 helix is conserved in insect and mammalian sodium channels (Du et al., 2013). In our model, G^{1k9} is exposed to the cytoplasm and may interact with a cytoplasmic part of the channel through a knob-into-hole contact. We expressed mutants $G^{1k9}A$ and $G^{1k9}I$ and found that they substantially decreased the channel sensitivity to pyrethroids (Fig. 4). We further expressed and tested two double mutations ($G^{1k9}A+I^{1k12}N$ and $G^{1k9}I+I^{1k12}N$), but did not find any synergistic effects of the mutations on the pyrethroid action (Fig. 4).

Discussion

Common and unique features of the initial and revised PyR1 models. The pioneering PyR1 model for the housefly sodium channel (O'Reilly et al., 2006) and *Drosophila*

Molecular Pharmacology Fast Forward. Published on May 13, 2015 as DOI: 10.1124/mol.115.098707
This article has not been copyedited and formatted. The final version may differ from this version.

sodium channel (Usherwood et al., 2007) and the revised PyR1 model elaborated in this study for the $AaNa_v1$-1 channel have several common features. These include the location of the receptor site in the II/III domain interface, extended conformation of the receptor-bound DMT, and direct contacts of DMT with seven experimentally determined pyrethroid sensing residues in helices IIL45 (M^{2k11}), IIS5 (L^{2o6}, T^{2o10} and L^{2o13}) and IIIS6 (F^{3i13}, F^{3i16} and F^{3i17}). However, there are four main differences between the initial and revised PyR1 models. First, in the initial model, DMT binds at the protein surface and interacts with three helices (IIL45, IIS5, and IIIS6), whereas in our revised model DMT binds deeply in the domain interface (Fig. 2F) and interacts with four helices (IIL45, IIS5, IIS6 and IIIS6). Second, dibromoethenyl and diphenylether moieties of DMT bound in the initial PyR1 model are oriented in the extra- and intracellular directions, respectively, whereas in the revised PyR1 model these moieties are oriented in the reversed way. Third, in the initial PyR1 model, DMT interacts with C^{2o14} in the middle part of IIS5 (Usherwood et al., 2007), whereas in the revised PyR1 model C^{2o14} is rather far from the ligand. Finally, in the revised PyR1 model, DMT interacts with L^{2k7} in the middle part of the IIL45 helix, whereas the original PyR1 model, this residue appears far from the ligand.

Some features of the revised DMT-bound PyR1 model were predetermined by the fact that we imposed two distance constraints to direct dibromoethenyl and diphenylether moieties towards L^{2k7} and V^{2i18}, respectively. These constraints forced DMT to adopt in PyR1 orientation analogous to that of PyR2-bound DMT whose dibromoethenyl and diphenylether moieties interact with I^{1k7} and L^{1i18}, respectively. Such orientation of the bound DMT was found optimal in the systematic exploration of different possibilities in modeling PyR2 (Du et al., 2013). The above two distance constraints biased overall orientation of DMT in PyR1 in only the first stage of MCM docking, whereas all specific DMT-PyR1 contacts were found in the subsequent stages of MCM docking that did not involve any ligand-channel distance constraints. It should also be

Molecular Pharmacology Fast Forward. Published on May 13, 2015 as DOI: 10.1124/mol.115.098707
This article has not been copyedited and formatted. The final version may differ from this version.

noted that the initial PyR1 model was built based on experimental data available by 2006, while our revised PyR1 model was built using experimental data available as of 2014 (Fig. 3).

Some mutations within PyR1 and PyR2 increased the potency of pyrethroids. Usually substitutions of pyrethroid-sensing residues decrease potency of pyrethroids, but there are intriguing exceptions. In our experiments, mutations $V^{2i12}A$ and $V^{2i12}L$ within PyR2 did not decrease potency of either PMT or DMT, but appear to slightly increase potency of both PMT and DMT (Fig. 4 and Table 1). In our PyR2 model, V^{2i12} is exposed towards I^{1o10} (Fig. 2E) and both residues may control the DMT access to PyR2. In earlier experiments, we found similar effects of increasing DMT and PMT potency in the analogous $I^{3i12}A$ mutation in PyR1 of the cockroach sodium channel (Du et al., 2009). In our revised PyR1 model, I^{3i12}, like V^{2i12}, extends towards T^{2o10}, and both residues may control access of DMT to PyR1 (Fig. 2F). Alanine substitutions of the bulky beta-branched residues I^{3i12} or V^{2i12} could widen the access path for pyrethroids from the membrane to reach the receptors and thus increase rather than decrease the channel sensitivity to pyrethroids. Substitution of the beta-branched V^{2i12} by a bigger, but more flexible leucine may also facilitate the ligand access to PyR2 and our data are consistent with this proposition (Fig. 4). The opposite leafs of the gates that separate PyR1 and PyR2 from lipids contain beta-branched T^{2o10} and I^{1o10}, respectively. We are not aware of alanine substitutions of these residues, but substitutions $T^{2o10}I$ or $I^{1o10}C$ by bigger residues decrease the ligands potency (Table 1) which may be explained in our models of PyR1 and PyR2 by a more restricted access path for pyrethroids from the membrane to their receptors.

$V^{2i12}A$ and $V^{2i12}L$ are putative kdr mutations in PyR2, which are found to coexist with kdr mutations $M^{2k11}L$ and $L^{2i16}S$ in pyrethroid-resistant populations of *Thrips tabaci* (Wu et al., 2013) and *Anopheles culicifacies* (Singh et al., 2010). Importantly, $M^{2k11}L$ and $L^{2i16}S$ significantly reduce channel sensitivity to pyrethroids (Table 1), and we suggest that the double mutations may have synergistic effects due to decreasing the ligand-channel interactions and facilitating

Molecular Pharmacology Fast Forward. Published on May 13, 2015 as DOI: 10.1124/mol.115.098707
This article has not been copyedited and formatted. The final version may differ from this version.

the ligand egress from PyR1 and PyR2. Another residue that may control access of pyrethroids to PyR2 is C^{2o14}. Mutation $C^{2o14}A$ decreases potency of DMT, but increases potency of PMT (Table 1). In our model, C^{2o14} is rather far from PyR1-bound DMT, but it interacts with T^{2o10} and thus may indirectly control access of pyrethroids to PyR1 (Fig. 2F).

How mutations beyond PyR1 and PyR2 can affect action of pyrethroids? Many known kdr mutations are located beyond the PyR1 and PyR2 sites. Some kdr mutations are found around PyR1 and PyR2, but respective residues do not interact with DMT molecules in our model. One mutation, $I^{1k12}N$, was found in pyrethroid resistant *Drosophila melanogaster* (Pittendrigh et al., 1997). We expressed the $I^{1k12}N$ mutant in oocytes and found significant reduction in the pyrethroid sensitivity of $I^{1k12}N$ mutant channels (Rinkevich et al., 2015). In our model, I^{1k12} is located at the face of the IL45 helix, which is opposite to the face that contains pyrethroid-sensing residues L^{1k7} and V^{1k11}. Simultaneous binding of DMT to L^{1k7}, V^{1k11} and I^{1k12} would be possible only if the ligand wraps around the linker-helix IL45 or if segment IL45 has a non-helical secondary structure. The first scenario is inconsistent with all the published models of pyrethroid binding, whereas the second scenario is inconsistent with the X-ray structures of sodium and potassium channel where the L45 helices are resolved. This implies an allosteric effect of the $I^{1k12}N$ mutation on the pyrethroid action. Possible mechanisms could be certain deformation of the helical structure of the IL45 linker by $I^{1k12}N$ or disruption of interaction of the linker with hydrophobic residues at a cytoplasmic part of the channel, which is beyond our model.

Rotational symmetry of PyR1 and PyR2. Figures 2C and D illustrate rotational symmetry of PyR1 and PyR2. Thus, clockwise rotation by 90 degrees of the cytoplasmic view (Fig. 2D) would put PyR1 in place of PyR2. To some extent, the symmetric disposition of ligands in PyR1 and PyR2 was imposed due to the biased docking of DMT to L^{2k7} and V^{2i18}. However, the docking predicted three new residues in PyR1 (F^{2i22}, L^{2i25} and L^{2i26}) and mutational analysis

Molecular Pharmacology Fast Forward. Published on May 13, 2015 as DOI: 10.1124/mol.115.098707
This article has not been copyedited and formatted. The final version may differ from this version.

confirmed these predictions (Fig. 4). The symmetric positions of pyrethroid-sensing residues in PyR1 and PyR2 are also illustrated in Table 1 and Figure 1. Figure 1 highlights pyrethroid-sensing residues that according to mutational analysis contribute to PyR1 (bold and highlighted) and PyR2 (bold and underlined). A total of eleven residues in PyR1 have matches in PyR2 (Table 1), and the majority of residues in these matching positions are hydrophobic, but structurally different amino acids.

Mutational analysis also confirmed several new pyrethroid-sensing residues in PyR2 (Fig. 4). Of course, the symmetry of PyR1 and PyR2 is not ideal due to sequence differences of the four channel repeat domains. For example, we observed a significant decrease in the potency of DMT and PMT in the kdr mutant $N^{2i15}S$. In our model N^{2i15} is close to the terminal phenyl ring of PyR2-bound DMT (Fig. 2A). Mutation $S^{3i15}A$ in the matching position of PyR1 has only a small effect on the DMT and PMT action (Du et al., 2009). This is consistent with our model in which the small side chain of S^{3i15} is farther from PyR1-bound DMT than the sidechain of N^{2i15} from the PyR2-bound DMT.

Mutation $L^{2o6}I$ in PyR1 decreases the sensitivity of sodium channels to DMT and PMT, whereas mutations $L^{1o6}I/A$ in the matching position of PyR2 had no effect on pyrethroid sensitivity (Table 1). Our model predicts that L^{2o6} and L^{1o6} control the ligand access to PyR1 and PyR2, respectively (Fig. 2E,F) and also directly interact with the receptor-bound pyrethroids. The combined effects of these two factors may depend on peculiarities of the amino acid substitutions. In addition, mutation $L^{2i25}A$ in PyR1 was very resistant to both DMT and PMT, whereas mutation $I^{1i25}A$ in the matching position of PyR2 had no effect on the action of pyrethroids (Table 1). The cause of this asymmetry is less clear.

In our model, the nitrile groups of DMT molecules approach conserved asparagines N^{3i20} in PyR1 and N^{2i20} in PyR2 (Fig. 2A,B). These asparagines are predicted to form interdomain H-bonds with polar residues in positions *2i29* and *1i29*, respectively (Tikhonov et al., 2015).

Molecular Pharmacology Fast Forward. Published on May 13, 2015 as DOI: 10.1124/mol.115.098707
This article has not been copyedited and formatted. The final version may differ from this version.

Mutation $N^{3i20}A$ in PyR1 decreases sensitivity of the cockroach sodium channel to pyrethroids (Du et al., 2009). Mutation $N^{2i20}A$ in PyR2 did not change the channel sensitivity to pyrethroids, but mutation $S^{1i29}A$ of the putative H-bonding partner of N^{2i20} did (Fig. 4) implying that the nitrile group of PyR2-bound DMT is closer to S^{1i29} than to N^{2i20}.

Molecular Pharmacology Fast Forward. Published on May 13, 2015 as DOI: 10.1124/mol.115.098707
This article has not been copyedited and formatted. The final version may differ from this version.

Conclusions

In this study, we further elaborated the dual-pyrethroid receptor paradigm by creating an atomic model of the mosquito sodium channel with two DMT molecules bound to two different receptors, PyR1 and PyR2 and performing model-driven mutagenesis in PyR1 and PyR2. Our models and experimental data predict a significant degree of rotational symmetry between the two pyrethroid receptor sites, though with subtle differences. In conjunction with findings from previous studies, our results suggest that simultaneous binding of pyrethroids to two receptor sites in the pore module of the insect sodium channel may be necessary to effectively lock the channel in the open state.

Molecular Pharmacology Fast Forward. Published on May 13, 2015 as DOI: 10.1124/mol.115.098707
This article has not been copyedited and formatted. The final version may differ from this version.

Acknowledgements

We thank Dr. Kris Silver for critical review of this manuscript. Computations were performed using the facilities of the Shared Hierarchical Academic Research Computing Network (SHARCNET, www.sharcnet.ca).

Molecular Pharmacology Fast Forward. Published on May 13, 2015 as DOI: 10.1124/mol.115.098707
This article has not been copyedited and formatted. The final version may differ from this version.

Authorship Contributions

Participated in research design: Zhorov and Dong

Conducted experiments and performed data analysis: Du, Nomura and Zhorov

Wrote or contributed to the writing of the manuscript: Du, Zhorov and Dong

Molecular Pharmacology Fast Forward. Published on May 13, 2015 as DOI: 10.1124/mol.115.098707
This article has not been copyedited and formatted. The final version may differ from this version.

References

(WHO) WHO (2007) Insecticide-treated mosquito nets: a WHO position statement, WHO, Geneva.

Bloomquist JR (1996) Ion channels as targets for insecticides. *Ann Rev Entomol* **41**(1):163-190.

Brengues C, Hawkes N, Chandre F, McCarroll L, Duchon S, Guillet P, Manguin S, Morgan J and Hemingway J (2003) Pyrethroid and DDT cross-resistance in *Aedes aegypti* is correlated with novel mutations in the voltage-gated sodium channel gene. *Med Vet Entomol* **17**(1):87-94.

Catterall WA (2012) Voltage-gated sodium channels at 60: structure, function and pathophysiology. *J Physiol* **590**(11):2577-2589.

Davies TG, Field LM, Usherwood PN and Williamson MS (2007) DDT, pyrethrins, pyrethroids and insect sodium channels. *IUBMB Life* **59**(3):151-162.

Dong K, Du Y, Rinkevich F, Nomura Y, Xu P, Wang L, Silver K and Zhorov BS (2014) Molecular biology of insect sodium channels and pyrethroid resistance. *Insect Biochem Mol Biol* **50**:1-17.

Du Y, Lee JE, Nomura Y, Zhang T, Zhorov BS and Dong K (2009) Identification of a cluster of residues in transmembrane segment 6 of domain III of the cockroach sodium channel essential for the action of pyrethroid insecticides. *Biochem J* **419**(2):377-385.

Du Y, Nomura Y, Satar G, Hu Z, Nauen R, He SY, Zhorov BS and Dong K (2013) Molecular evidence for dual pyrethroid-receptor sites on a mosquito sodium channel. *Proc Natl Acad Sci U S A* **110**(29):11785-11790.

Endersby NM, Viduka K, Baxter SW, Saw J, Heckel DG and McKechnie SW (2011) Widespread pyrethroid resistance in Australian diamondback moth, *Plutella xylostella* (L.), is related to multiple mutations in the para sodium channel gene. *Bull Entomol Res* **101**(4):393-405.

Garden DP and Zhorov BS (2010) Docking flexible ligands in proteins with a solvent exposure- and distance-dependent dielectric function. *J Comput Aided Mol Des* **24**(2):91-105.

Guerrero F, Jamroz R, Kammlah D and Kunz S (1997) Toxicological and molecular characterization of pyrethroid-resistant horn flies, *Haematobia irritans*: identification of *kdr* and *super-kdr* point mutations. *Insect Biochem Mol Biol* **27**(8-9):745-755.

He H, Chen A, Davey R, Ivie G and George J (1999) Identification of a point mutation in the *para*-type sodium channel gene from a pyrethroid-resistant cattle tick. *Biochem Biophys Res Commun* **261**(3):558-561.

Kawada H, Higa Y, Komagata O, Kasai S, Tomita T, Yen NT, Loan LL, Sánchez RAP and Takagi M (2009) Widespread distribution of a newly found point mutation in voltage-gated sodium channel in pyrethroid-resistant *Aedes aegypti* populations in Vietnam. *PLoS NeglTrop Dis* **3**(10):e0000527.

Kwon DH, Clark JM and Lee SH (2010) Cloning of a sodium channel gene and identification of mutations putatively associated with fenpropathrin resistance in *Tetranychus urticae*. *Pestic Biochem Physiol* **97**(2):93-100.

Li Z and Scheraga HA (1987) Monte Carlo-minimization approach to the multiple-minima problem in protein folding. *Proc Natl Acad Sci USA* **84**(19):6611-6615.

Long SB, Campbell EB and Mackinnon R (2005) Crystal structure of a mammalian voltage-dependent Shaker family K^+ channel. *Science* **309**(5736):897-903.

Morin S, Williamson MS, Goodson SJ, Brown JK, Tabashnik BE and Dennehy TJ (2002) Mutations in the *Bemisia tabaci para* sodium channel gene associated with resistance to a pyrethroid plus organophosphate mixture. *Insect Biochem Molec Biol* **32**:1781-1791.

Narahashi T (1986) Mechanisms of action of pyretrhoids on sodium and calcium channel gating, in *Neuropharmacology and Pesticide Action* (Ford MG, Usherwood PNR, Reay RC and Lunt GG eds) pp 36-60, Ellis Horwood, Chichester, England.

Narahashi T (1996) Neuronal ion channels as the target sites of insecticides. *Pharmacol Toxicol* **79**(1):1-14.

O'Reilly AO, Khambay BP, Williamson MS, Field LM, Wallace BA and Davies TG (2006) Modelling insecticide-binding sites in the voltage-gated sodium channel. *Biochem J* **396**(2):255-263.

Pittendrigh B, Reenan R, ffrench-Constant RH and Ganetzky B (1997) Point mutations in the *Drosophila* sodium channel gene para associated with resistance to DDT and pyrethroid insecticides. *Mol Gen Genet* **256**(6):602-610.

Pridgeon JW, Appel AG, Moar WJ and Liu N (2002) Variability of resistance mechanisms in pyrethroid resistant German cockroaches (Dictyoptera: Blattellidae). *Pestic Biochem Physiol* **73**(3):149-156.

Rinkevich FD, Du Y, Tolinski J, Ueda A, Wu CF, Zhorov BS and Dong K (2015) Distinct Roles of the DmNa and DSC1 Channels in the Action of DDT and Pyrethroids. *Neurotoxicology* **47**:99-106.

Rinkevich FD, Du YZ and Dong K (2013) Diversity and convergence of sodium channel mutations involved in resistance to pyrethroids and DDT. *Pestic Biochem Physiol* **106**(3):93-100.

Singh OP, Dykes CL, Das MK, Pradhan S, Bhatt RM, Agrawal OP and Adak T (2010) Presence of two alternative kdr-like mutations, L1014F and L1014S, and a novel mutation, V1010L, in the voltage gated Na^+ channel of *Anopheles culicifacies* from Orissa, India. *Malaria J* **9**:146.

Soderlund D (2005) Sodium channels, in *Comprehensive Molecular Insect Science* (Gilbert LI, Latrou K and Gill SS eds) pp 1-24, Elsevier, B V, New York.

Soderlund DM (2010) State-dependent modification of voltage-gated sodium channels by pyrethroids. *Pestic Biochem Physiol* **97**(2):78-86.

Tan J, Liu Z, Wang R, Huang ZY, Chen AC, Gurevitz M and Dong K (2005) Identification of amino acid residues in the insect sodium channel critical for pyrethroid binding. *Mol Pharmacol* **67**(2):513-522.

Tan WL, Li CX, Wang ZM, Liu MD, Dong YD, Feng XY, Wu ZM, Guo XX, Xing D, Zhang YM, Wang ZC and Zhao TY (2012) First detection of multiple knockdown resistance (*kdr*)-like mutations in voltage-gated sodium channel using three new genotyping methods in *Anopheles sinensis* from Guangxi Province, China. *J Med Entomol* **49**(5):1012-1020.

Tatebayashi H and Narahashi T (1994) Differential mechanism of action of the pyrethroid tetramethrin on tetrodotoxin-sensitive and tetrodotoxin-resistant sodium channels. *J Pharmacol Exp Ther* **270**(2):595-603.

Tikhonov DB, Bruhova I, Garden DP and Zhorov BS (2015) State-dependent inter-repeat contacts of exceptionally conserved asparagines in the inner helices of sodium and calcium channels. *Pflugers Arch* **467**(2):253-266.

Usherwood PNR, Davies TGE, Mellor IR, O'Reilly AO, Peng F, Vais H, Khambay BPS, Field LM and Williamson MS (2007) Mutations in DIIS5 and the DIIS4-S5 linker of *Drosophila melanogaster* sodium channel define binding domains for pyrethroids and DDT. *Febs Letters* **581**(28):5485-5492.

Wu M, Gotoh H, Waters T, Walsh DB and Lavine LC (2014) Identification of an alternative knockdown resistance (*kdr*)-like mutation, M918L, and a novel mutation, V1010A, in the *Thrips tabaci* voltage-gated sodium channel gene. *Pest Manag Sci* **70**(6):977-981.Zhorov BS and Tikhonov DB (2004) Potassium, sodium, calcium and glutamate-gated channels: pore architecture and ligand action. *J Neurochem* **88**(4):782-799.

Molecular Pharmacology Fast Forward. Published on May 13, 2015 as DOI: 10.1124/mol.115.098707
This article has not been copyedited and formatted. The final version may differ from this version.

Footnotes

KD and BSZ are joint senior authors. This study was supported by the National Institutes of Health National Institute of General Medical Sciences [GM057440] and the Natural Sciences and Engineering Research Council of Canada [RGPIN-2014-04894].

Molecular Pharmacology Fast Forward. Published on May 13, 2015 as DOI: 10.1124/mol.115.098707
This article has not been copyedited and formatted. The final version may differ from this version.

Figure Legends

Figure 1. Aligned sequences of $K_v1.2$ and $AaNa_v1$-1 channels indicating residues that are predicted to contribute to PyR1 or PyR2 or control ligand access to PyR1 or PyR2. PyR1 residues are highlighted and PyR2 residues are underlined. Substitutions of these residues have been tested experimentally previously or in this study (Table 1).

Figure 2. $K_v1.2$-based model of the open $AaNa_v1$-1 channel pore module with two DMT molecules docked into PyR2 and revised PyR1 sites. Helices in domains I, II, III and IV are shown by pink, yellow, green and white ribbons, respectively. Known pyrethroid-sensing residues are shown as sticks. (A) Side view of the PyR2 model along helix IIS6. (B) Side view of the PyR1 model along helix IIIS6. (C and D) side and cytoplasmic views of the $AaNa_v1$-1 channel model with two DMT molecules (space-filled). (E and F) PyR2 and PyR1 models where residues that control access of the ligands to the receptors are shown by semi-transparent surfaces. Note the deep location of DMT molecules in the domain interfaces. Significant "breathing" of the channel backbones and conformational flexibility of the residues that control the access of pyrethroid ligands from the membrane to their receptors are necessary for pyrethroid binding.

Figure 3 Topology of the $AaNa_v1$-1a sodium channel. (A) Pyrethroid-sensing residues are indicated for PyR1 (open circles) and PyR2 (gray circles), respectively. Mutations that are detected in pyrethroid-resistant field populations are underlined. (B) Mutations tested in our study. Previously discovered kdr mutations are underlined. Open and solid circles indicate mutations within or nearby PyR1 and PyR2, respectively.

Molecular Pharmacology Fast Forward. Published on May 13, 2015 as DOI: 10.1124/mol.115.098707
This article has not been copyedited and formatted. The final version may differ from this version.

Figure 4. Pyrethroid sensitivity of $AaNa_v1$-1 and its mutants. Percentage of the channel modification by 1.0 μM DMT (A) or 1.0 μM PMT (B) was determined by the method of Tatebayashi and Narahashi (Tatebayashi and Narahashi, 1994). The number of oocytes for each mutant construct was > 5. Error bars indicate mean ± s.e.m. The asterisks indicate significant difference from the $AaNa_v1$-1 channel as determined by using one-way analysis of variance with Scheffé's post hoc analysis, and significant values were set at $p<0.05$. Representative tail current traces from $AaNa_v1$-1 channels in the presence of 0.1 μM and 1.0 μM of DMT or PMT, and the most resistant mutant channel, $L^{2i25}A$, in the presence of 1.0 μM and 10 μM of DMT or PMT are shown below the histograms.

The caption for the pdb file: Kv1.2-based model of the open $AaNa_v1$-1 channel pore module with two DMT molecules in the PyR2 and revised PyR1 sites.

Molecular Pharmacology Fast Forward. Published on May 13, 2015 as DOI: 10.1124/mol.115.098707
This article has not been copyedited and formatted. The final version may differ from this version.

Table 1. Effects of mutations within the two pyrethroid receptor sites on the action of DMT and PMT. Symbols ↓, ↑, and ≈ indicate decrease, increase, or insignificant change of the ligand potency, respectively.

PyR1				PyR2			
Mutant	Ref.[a]	DMT	PMT	Mutant	Ref.[a]	DMT	PMT
$L^{2k7}F/I$	1	↓/↓	≈ /↑	$I^{1k7}A$	3	↓	↓
$M^{2k11}T$	1	↓	↓	$V^{1k11}A$	3	↓	↓
				$S^{1o2}A$	5	↓	↓
$L^{2o6}I$	1	↓	↓	$L^{1o6}I/A$	3,5	↑/≈	≈/↑
$T^{2o10}I$	1	↓	↓	$I^{1o10}C$	3	↓	↓
$L^{2o13}F$	1	↓	≈	$T^{1o13}W$	3	≈	≈
$C^{2o14}A$	1	↓	↑				
$V^{2i18}G$	3	↓	↓	$L^{1i18}G$	3	↓	↓
$F^{2i22}S$ [b]	5	↓	↓	$I^{1i22}A$	5	↓	↓
$L^{2i25}A$	5	↓	↓	$I^{1i25}A$	5	≈	≈
$L^{2i26}A$	5	↓	↓				
				$S^{1i29}A$	5	↓	↓
$I^{3i12}A$	2	↑	↑	$V^{2i12}A/L$	5	≈/↑	↑/↑
$F^{3i13}C$	3	↓	↓	$I^{2i13}M$	3	≈	↓
$S^{3i15}A$	2	≈	≈	$N^{2i15}S$	5	↓	↓
$F^{3i16}A$	2	↓	↓	$L^{2i16}F/S$	3	↓/↓	↓/↓
$F^{3i17}I$	4	↓	↓				
$N^{3i20}A$	2	↓	↓	$N^{2i20}A$	5	≈	≈

[a] References: 1, (Usherwood et al., 2007); 2 (Du et al., 2009); 3 (Du et al., 2013) and references therein; 4 (Tan et al., 2005); 5, This study (Fig. 3B and 4).

[b] F^{2i22} contributes to both PyR1 and PyR2.

Molecular Pharmacology Fast Forward. Published on May 13, 2015 as DOI: 10.1124/mol.115.098707
This article has not been copyedited and formatted. The final version may differ from this version.

Table 2. Voltage dependence of activation and inactivation of mosquito sodium channels

Na+ Channel Type	Activation		Inactivation	
	$V_{1/2}$ (mV)	k (mV)	$V_{1/2}$ (mV)	k (mV)
$AaNa_v1$-1	-29.2 ± 0.8	5.2 ± 0.3	-52.9 ± 0.4	4.9 ± 0.2
$G^{1K9}A$	-32.6 ± 1.2	5.0 ± 0.2	-51.9 ± 0.4	4.8 ± 0.1
$G^{1K9}I$	-32.8 ± 1.4	6.3 ± 0.6	-52.8 ± 1.2	4.6 ± 0.2
$I^{1k12}N$	-33.8 ± 0.9	5.1 ± 0.4	-51.8 ± 0.6	4.6 ± 0.1
$I^{1k12}N$+ $G^{1K9}A$	-30.2 ± 1.0	5.5 ± 0.3	-55.5 ± 0.8	4.8 ± 0.3
$I^{1k12}N$+ $G^{1K9}I$	-30.4 ± 0.5	6.2 ± 0.2	-55.5 ± 1.1	5.1 ± 0.2
$S^{1o2}A$	-32.9 ± 0.2	5.1± 0.1	-54.0 ± 0.4	4.5 ± 0.1
$N^{1o5}A$	-33.5 ± 0.8	4.5 ± 0.2	-52.1 ± 0.6	4.5 ± 0.1
$L^{1o6}A$	-50.5 ± 1.8*	6.1 ± 0.6	-64.7 ± 0.7*	6.4 ± 0.3
$R^{1o7}A$	-31.0 ± 0.6	5.1 ± 0.3	-53.9 ± 0.7	5.1 ± 0.1
$I^{1i22}A$	-34.3 ± 1.1	5.5 ± 0.4	-52.9 ± 0.5	5.0 ± 0.1
$I^{1i25}A$	-30.0 ± 0.8	7.0 ± 0.6	-67.5 ± 0.8*	5.0 ± 0.1
$S^{1i29}A$	-33.0 ± 0.8	5.5 ± 0.4	-54.8 ± 0.5	5.1 ± 0.1
$V^{2i12}A$	-26.7 ± 0.7	5.6 ± 0.4	-53.5 ± 0.8	5.5 ± 0.1
$V^{2i12}L$	-32.7 ± 0.8	5.5 ± 0.1	-50.9 ± 0.5	4.8 ± 0.1
$N^{2i15}S$	-28.8 ± 1.3	5.1 ± 0.1	-52.9 ± 1.4	4.9 ± 0.2
$N^{2i20}A$	-30.8 ± 0.6	5.4 ± 0.2	-58.7 ± 0.5	5.3± 0.1
$F^{2i22}S$	-30.7 ± 0.9	5.3 ± 0.7	-51.3 ± 0.9	4.7 ± 0.1
$L^{2i25}A$	-28.5 ± 0.8	5.9 ± 0.3	-51.5 ± 0.8	4.8 ± 0.1
$L^{2i26}A$	-31.7 ± 1.1	7.2 ± 0.4	-63.1 ± 1.2*	6.0 ± 0.4

The voltage dependences of conductance and inactivation were fitted with a two-state Boltzmann equation to determine $V_{1/2}$, the voltage for half- maximal conductance or inactivation, and k, the slope factor for conductance or inactivation. The values in the table represent the mean ± S.E.M and the number of oocytes was 6-16. The asterisks indicate significant differences as determined by one-way ANOVA ($p<0.05$) with Scheffe's post hoc analysis.

Figure 1

Channel	Segment	#	k1 | k11 o1 | o11 | o21 |
K_v1.2	L45-S5	323	SKGLQILGQT LK ASMRELGLLI FFLFIGVILF SSAVYFAE
$AaNa_v$1-1	IL45-S5	281	VPGLKT**I**VGA **V**I E**S**VKN**L**RDV**I** IITMFSLSVF ALMGLQIY
	IIL45-S5	917	WPTLNL**L**ISI **M**G RTMGA**L**GNL**T** FV**LC**IIIFIF AVMGMQLF
	IIIL45-S5	1419	MQGMRVVVNA LV QAIPSIFNVL LVCLIFWLIF AIMGVQLF
	IVL45- S5	1737	AKGIRTLLFA LA MSLPALFNIC LLLFLVMFIF AIFGMSFF
			i1 | i11 | i21 |
K_v1.2	S6	385	IGGKIVGSLC AIAGVLTIAL PVPVIVSNFN
$AaNa_v$1-1	IS6	429	PWHMLFFIVI IFLGSFY**L**VN L**I**LA**I**VAM**S**Y
	IIS6	1006	VSCIPFFLAT V**VI**G**NL**V**V**L**N** L**F**LA**LL**LSNF
	IIIS6	1540	IYMYLYFVFF II**F**GS**FF**TL**N** LFIGVIIDNF
	IVS6	1840	TIGITYLLAY LVISFLIVIN MYIAVILENY

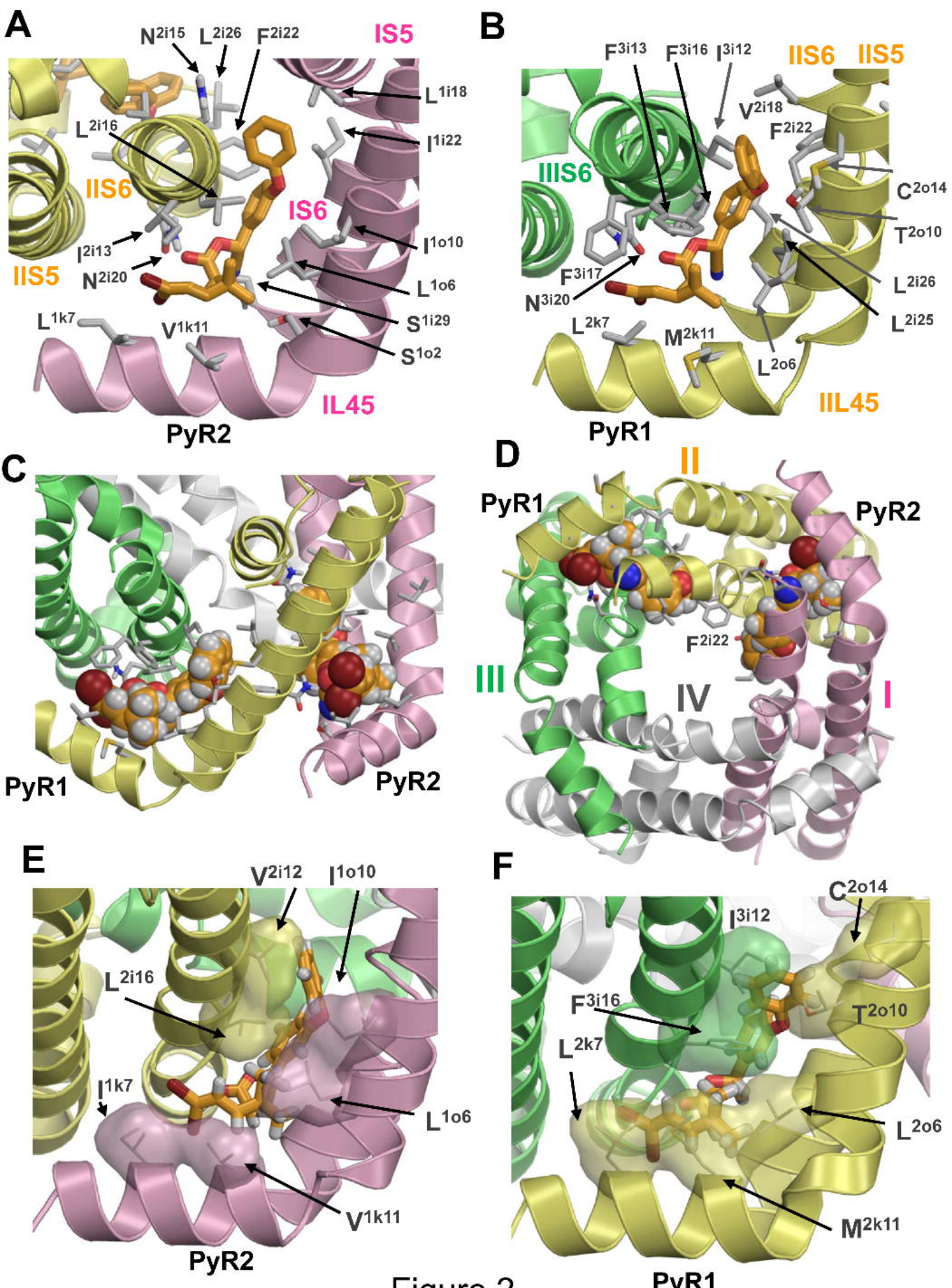
A
N2i15
L2i26
F2i22
IS5
L1i18
L2i16
I1i22
IIS6
IS6
I1o10
I2i13
IIS5
N2i20
L1o6
S1i29
L1k7
V1k11
S1o2
IL45
PyR2
B
F3i13
F3i16
I3i12
IIS6
IIS5
V2i18
F2i22
IIIS6
C2o14
T2o10
F3i17
L2i26
N3i20
L2i25
L2k7
M2k11
L2o6
IIL45
PyR1
C
PyR1
PyR2
D
II
PyR1
PyR2
F2i22
III
IV
I
E
V2i12
I1o10
L2i16
I1k7
L1o6
V1k11
PyR2
F
C2o14
I3i12
F3i16
T2o10
L2k7
L2o6
M2k11
PyR1

Figure 2

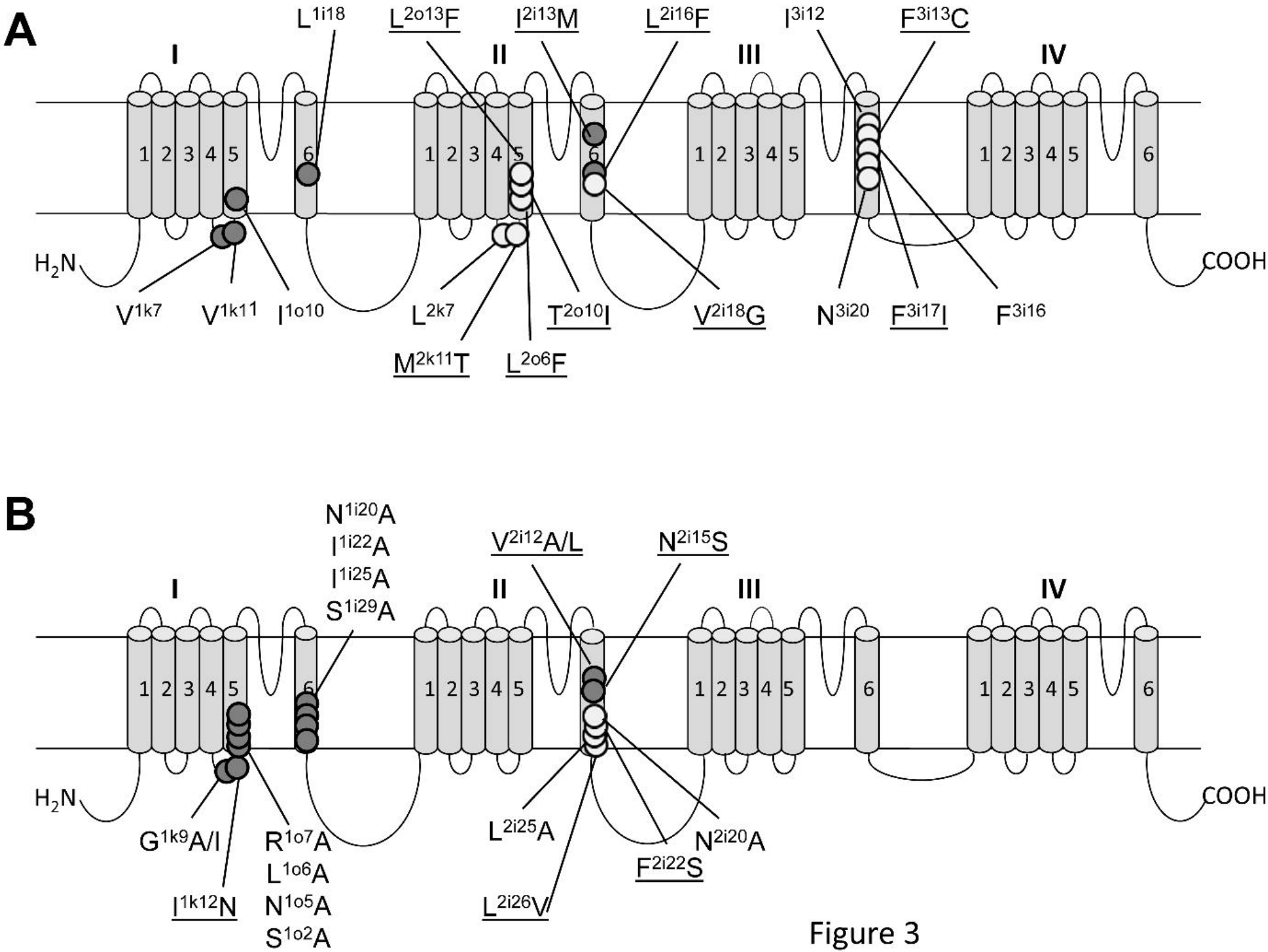
A
I
II
III
IV
1 2 3 4 5 6
H2N
COOH
L1i18
L2o13F
I2i13M
L2i16F
I3i12
F3i13C
V1k7
V1k11
I1o10
L2k7
T2o10I
V2i18G
N3i20
F3i17I
F3i16
M2k11T
L2o6F
B
N1i20A
I1i22A
I1i25A
S1i29A
V2i12A/L
N2i15S
G1k9A/I
R1o7A
L1o6A
N1o5A
S1o2A
I1k12N
L2i25A
N2i20A
F2i22S
L2i26V

Figure 3

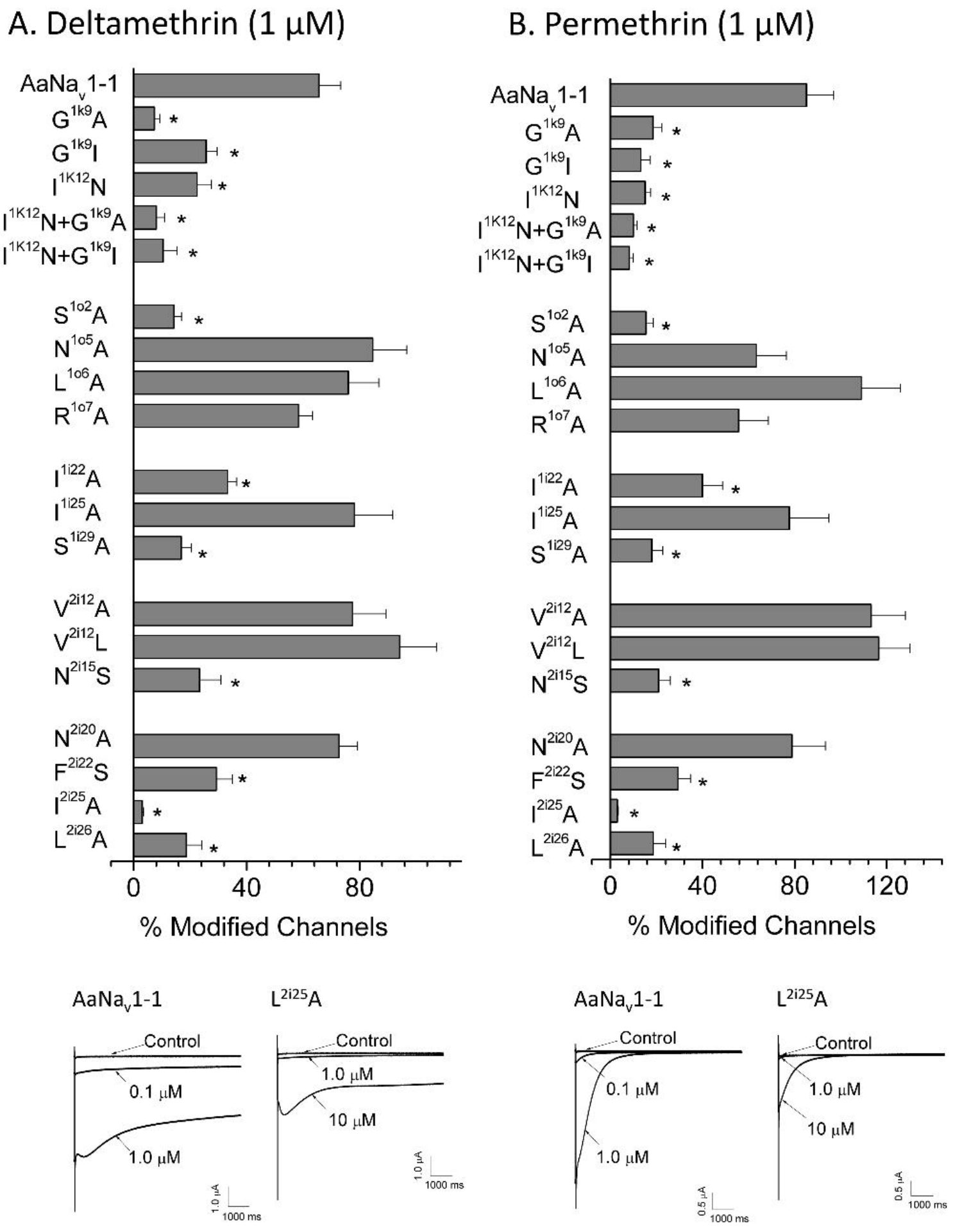
A. Deltamethrin (1 μM)
B. Permethrin (1 μM)
AaNav1-1
G1k9A
G1k9I
I1K12N
I1K12N+G1k9A
I1K12N+G1k9I
S1o2A
N1o5A
L1o6A
R1o7A
I1i22A
I1i25A
S1i29A
V2i12A
V2i12L
N2i15S
N2i20A
F2i22S
I2i25A
L2i26A
0
40
80
120
% Modified Channels
AaNav1-1
L2i25A
Control
0.1 μM
1.0 μM
10 μM
1.0 μA
1000 ms
0.5 μA

Figure 4